

Mechanisms for extraordinary optical transmission through bull's eye structures

S. Carretero-Palacios,^{1,*} O. Mahboub,^{2,4} F. J. Garcia-Vidal,³
L. Martin-Moreno,¹ Sergio G. Rodrigo,¹ C. Genet,² and
T. W. Ebbesen²

¹*Instituto de Ciencia de Materiales de Aragon and Departamento de Fisica de la Materia Condensada, CSIC-Universidad de Zaragoza, E-50009, Zaragoza, Spain,*
²*ISIS, Université de Strasbourg and CNRS, UMR 7006, 8 allée G. Monge, 67000 Strasbourg, France*

³*Departamento de Fisica Teorica de la Materia Condensada, Universidad Autonoma de Madrid, Madrid 28049, Spain*

⁴*o.mahboub@unistra.fr*

**sol@unizar.es*

Abstract: We analyze both experimentally and theoretically the physical mechanisms that determine the optical transmission through deep sub-wavelength bull's eye structures (concentric annular grooves surrounding a circular hole). Our analysis focus on the transmission resonance as a function of the distance between the central hole and its nearest groove. We find that, for that resonance, each groove behaves almost independently, acting as an optical cavity that couples to incident radiation, and reflecting the surface plasmons radiated by the other side of the same cavity. It is the constructive contribution at the central hole of these standing waves emitted by independent grooves which ends up enhancing transmission. Also for each groove the coupling and reflection coefficients for surface plasmons are incorporated into a phenomenological Huygens-Fresnel model that gathers the main mechanisms to enhance transmission. Additionally, it is shown that the system presents a collective resonance in the electric field that does not lead to resonant transmission, because the fields radiated by the grooves do not interfere constructively at the central hole.

© 2011 Optical Society of America

OCIS codes: (040.5160) Photodetectors; (050.1220) Apertures; (050.1950) Diffraction gratings; (120.7000) Transmission; (240.6680) Surface plasmons; (310.6628) Subwavelength structures, nanostructures.

References and links

1. C. Genet and T. W. Ebbesen, "Light in tiny holes," *Nature* **445**, 39-46 (2007).
2. F. J. Garcia-Vidal, L. Martin-Moreno, T. W. Ebbesen, and L. K. Kuipers, "Light passing through subwavelength apertures," *Rev. Mod. Phys.* **82**, 729787 (2010).
3. T. W. Ebbesen, H. L. Lezec, H. F. Ghaemi, T. Thio, and P. A. Wolff, "Extraordinary optical transmission through subwavelength hole arrays," *Nature* **391**, 667-669 (1998).
4. T. Thio, H. L. Lezec, T. W. Ebbesen, K. M. Pellerin, G. D. Lewen, A. Nahata, and R. A. Linke, "Giant optical transmission of subwavelength apertures: physics and applications," *Nanotechnology* **13**, 429-432 (2002).
5. H. J. Lezec, A. Degiron, E. Devaux, R. A. Linke, L. Martín-Moreno, F. J. García-Vidal, and T. W. Ebbesen, "Beaming light from a subwavelength aperture," *Science* **297**, 820-822 (2002).

6. F. I. Baida, D. V. Labeke, and B. Guizal, "Enhanced Confined Light Transmission by Single Subwavelength Apertures in Metallic Films," *Appl. Opt.* **42**, 68116815 (2003).
7. A. Degiron and T. Ebbesen, "Analysis of the transmission process through single apertures surrounded by periodic corrugations," *Opt. Express* **12**, 3694-3700 (2004).
8. A. Agrawal, H. Cao, and A. Nahata, "Time-domain analysis of enhanced transmission through a single subwavelength aperture," *Opt. Express* **13**, 3535-3542 (2005).
9. Z.-B. Li, J.-G. Tian, Z.-B. Liu, W.-Y. Zhou, and C.-P. Zhang, "Enhanced light transmission through a single subwavelength aperture in layered films consisting of metal and dielectric," *Opt. Express* **13**, 9071-9077 (2005).
10. O. Mahboub, S. C. Palacios, C. Genet, F. J. Garcia-Vidal, S. G. Rodrigo, L. Martín-Moreno, and T. W. Ebbesen, "Optimization of bull's eye structures for transmission enhancement," *Opt. Express* **18**, 11292-11299 (2010).
11. H. Ko, H. C. Kim, and M. Cheng, "Light focusing at metallic annular slit structure coated with dielectric layers," *Appl. Opt.* **49**, 950-954 (2010).
12. L.-L. Wang, X.-F. Ren, R. Yang, G.-C. Guo, and G.-P. Guo, "Transmission of doughnut light through a bulls eye structure," *Appl. Phys. Lett* **95**, 111111-111113 (2009).
13. T. Ishi, J. Fujikata, and K. Ohashi, "Large Optical Transmission through a Single Subwavelength Hole Associated with a Sharp-Apex Grating," *Jpn. J. Appl. Phys.* **44**, L170-L172 (2005).
14. X. C. G. Zheng and C. Yang, "Surface-wave-enabled darkfield aperture for background suppression during weak signal detection," *PNAS* **107**, 9043-9048 (2010).
15. G. Zheng and C. Yang, "Improving weak-signal identification via predetection background suppression by a pixel-level, surface-wave-enabled dark-field aperture," *Opt. Lett.* **35**, 2636-26348 (2010).
16. J. H. M. Consonni and G. Léronde, "Fabry-Perot type enhancement in plasmonic visible nanosource," *Appl. Phys. Lett.* **94**, 051105-1-051105-3 (2009).
17. L. Martín-Moreno, F. J. García-Vidal, H. J. Lezec, A. Degiron, and T. W. Ebbesen, "Theory of Highly Directional Emission from a Single Subwavelength Aperture Surrounded by Surface Corrugations," *Phys. Rev. Lett.* **90**, 167401-167404 (2003).
18. F. J. García-Vidal, H. J. Lezec, T. W. Ebbesen, and L. Martín-Moreno, "Multiple Paths to Enhance Optical Transmission through a Single Subwavelength Slit," *Phys. Rev. Lett.* **90**, 213901-213904 (2003).
19. C. K. Chang, D. Z. Lin, C. S. Yeh, C. K. Lee, Y. C. Chang, M. W. Lin, J. T. Yeh, and J. M. Liu, "Similarities and differences for light-induced surface plasmons in one- and two-dimensional symmetrical metallic nanostructures," *Opt. Lett.* **31**, 2341-2343 (2006).
20. P. D. Flammer, I. C. Schick, R. T. Collins, and R. E. Hollingsworth, "Interference and resonant cavity effects explain enhanced transmission through subwavelength apertures in thin metal films," *Opt. Express* **15**, 7984-7993 (2007).
21. O. T. A. Janssen, H. P. Urbach, and G. W. t' Hooft, "Giant optical transmission of a subwavelength slit optimized using the magnetic field phase," *Phys. Rev. Lett.* **99**, 043902-043905 (2007).
22. L. Wang, J.-X. Cao, Y. Lv, L. Liu, T.-Y. Niu, and Y.-C. Du, "Experimental study of surface-wave-assisted microwave transmission through a single subwavelength slit," *J. Appl. Phys.* **105**, 093115-093115-6 (2009b).
23. Y. Cui and S. He, "A theoretical re-examination of giant transmission of light through a metallic nano-slit surrounded with periodic grooves," *Opt. Express* **17**, 13995-14000 (2009).
24. L. Cai, G. Li, Z. Wang, and A. Xu, "Interference and horizontal Fabry-Perot resonance on extraordinary transmission through a metallic nanoslit surrounded by grooves," *Opt. Lett.* **35**, 127-129 (2010).
25. A. Roberts and R. McPhedran, "Bandpass grids with annular apertures," *IEEE Trans. Antennas Propag.* **36**, 607-611 (1988).
26. F. de León-Pérez, G. Brucoli, F. J. García-Vidal, and L. Martín-Moreno, "Theory on the scattering of light and surface plasmon polaritons by arrays of holes and dimples in a metal film," *New J. Phys.* **10**, 105017 (2008).
27. L. Martín-Moreno and F. J. García-Vidal, "Minimal model for optical transmission through holey metal films," *J. Phys.: Condens. Matter* **20**, 304214 (2008).
28. L. D. Landau, E. M. Lifshitz, and L. P. Pitaevskii, *Electrodynamics of Continuous Media* (Pergamon Press, New York, 1960).
29. E. D. Palik, *Handbook of optical constants of solids II* (Boston: Academic Press, 1991, edited by Palik, Edward D., 1991).
30. F. López-Tejeira, F. J. García-Vidal, and L. Martín-Moreno, "Scattering of surface plasmons by one-dimensional periodic nanoindented surfaces," *Phys. Rev. B (R)* **72**, 161405(R)-161408 (2005).
31. P. Lalanne and J. P. Hugonin, "Interaction between optical nano-objects at metallo-dielectric interfaces," *Nature Phys.* **2**, 551-556 (2006).
32. J.-Y. Laluet, E. Devaux, C. Genet, T. W. Ebbesen, J.-C. Weeber, and A. Dereux, "Optimization of surface plasmons launching from subwavelength hole arrays: modelling and experiments," *Opt. Express* **15**, 3488-3495 (2007).

1. Introduction

The Extraordinary Optical Transmission (EOT) through subwavelength apertures in metallic films [1,2] has received much attention since its first report [3]. In particular, periodic structures around a nano-aperture are of great interest because the optical transmittance through these systems can be largely tailored with respect to that of an isolated aperture. Bull's eye (BE) structures, consisting of a subwavelength aperture surrounded by annular grooves, have revealed that the transmitted light through the aperture can be strongly boosted and concentrated due to the excitation of surface plasmons (SP) launched by the periodic corrugations [4–13]. Attention has recently been given on coherent optical properties that are at play on BE structures where the direct transmission of light through the aperture interferes with an SP component launched by the corrugations. In this context, it has been realized that BEs can be carefully designed as to suppress any bright background in sensitive darkfield detection and imaging -so called SWEDA microscopy [14, 15]. When the periodic surrounding grating is designed as a Bragg reflector for the illumination wavelength, the BE structure behaves as a plasmonic micro-cavity around the hole, with strong potential in nanolithography and data storage [16]. Given these promises, it is important to discuss thoroughly the coherent properties of the BE structure, from both experimental and theoretical point of views. From a theoretical point of view, most works have considered the one dimensional version (1D, a slit surrounded by linear grooves) [17–24] which is both simpler to compute (due to the translational symmetry in one direction) and easier to analyze (in a periodic 1D system all grooves have the same electromagnetic response, while in the BE the response of each groove depends on its radius).

In this paper we go beyond the 1D analysis, providing a detailed description and analysis of BE transmission properties. By considering the interfering contributions of the direct transmission through the hole and the SP component in the transmission process, we reveal experimentally how the two contributions determine the transmission spectra of a BE. We also carry out numerical calculations accounting for the cylindrical symmetry of the BE system. This allows us to give analytical expressions for the most relevant parameters that determine the optical behavior of the BE. We find that the mechanism to enhance transmission is related to constructive interference at the central hole of standing SP waves independently emitted by each groove. Furthermore, a simple phenomenological model that gathers the main mechanisms to enhance transmission is provided.

2. Experimental results and phenomenological model

2.1. Experimental results

A schematic of a BE structure is displayed in Fig. 1(a). For all the following experiments, the structure is milled in a $h = 280\text{nm}$ thick Au film deposited on a glass substrate using focused ion beam (FIB) lithography technique. In order to obtain EOT in the optical regime, the distance between consecutive grooves (the “period”, p) is chosen as $p = 600\text{nm}$. Dimensions characterizing grooves and hole are in the subwavelength regime: all grooves have 90nm depth and 220nm width, and the radius of the central hole is $r_c = 125\text{nm}$. We consider $N = 6$ annular grooves, a typical number that fulfills the compromise between small structure size and high field enhancement [10]. The sample was illuminated from the corrugated side with collimated white light and the far-field transmission spectra were recorded with an optical microscope Nikon TE200, coupled to an Acton spectrometer and a Princeton Instruments CCD camera.

Figure 2(a) shows the transmission spectra measured as a function of the incident wavelength λ . The scale of colors in the figure is linear, and in arbitrary units. The figure shows the expected resonances at wavelengths slightly larger than the period (in this case $\lambda \approx 660\text{nm}$) [5, 17]. However, considering the possibility that additional coherent effects can modulate the optical

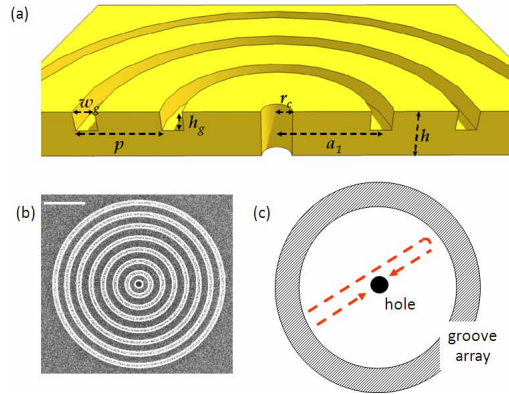


Fig. 1. (a) Schematic representation of a BE structure, consisting of a metal film of thickness h deposited on a glass substrate, perforated by a central hole with radius r_c and N concentric circular grooves (all with the same width w_g and depth h_g) separated by a period p . The variable distance between the hole the nearest groove is a_1 . (b) SEM image of a experimental structure milled by FIB lithography. The scale bar corresponds to $2\ \mu\text{m}$. (c) Sketch of the re-illumination SP component as implemented in the phenomenological model described in the text.

enhancement associated with these resonances, we have explored further the transmission dynamics by changing also the distance a_1 between the central hole and its nearest groove. When the spectra are displayed in the $\lambda - a_1$ parameter space, they clearly show that the resonant profile is modified as the distance a_1 is varied. In order to have a first understanding of this rather complex landscape, we have developed a simple phenomenological model that captures the main mechanisms playing a role at $\lambda = 660\text{nm}$.

2.2. Phenomenological model

To test the validity of the model compared to actual experiments, we consider the most simple situation of a normal incidence illumination of the BE. In its form, the model:

- treats the groove array as a resonant “black box” with an EM response characterized by a general *complex coupling coefficient*, γ , which gives the fraction of normally incident field amplitude that the groove array *locally* couples into SP,
- considers the central hole being illuminated by the incident EM field and re-illuminated by light coming from the array via SP,
- accounts for hole re-illumination as an SP-assisted two-path scattering process: (i) one direct path from the array to the hole and (ii) and a secondary path corresponding to SP back reflected by the groove array to the central hole with *complex reflection amplitude* r (see a schematic representation in Fig. 1(c)),
- assumes that the hole is sufficiently small so that the illumination of the hole (by either the incident EM field or the light coming from the array) depends only on the field amplitude and not on the parallel wavevector. In this case, the transmittance through the hole, can be expressed as $T = T_{SH} |F_{array}|^2$, where T_{SH} is the transmission of light through a single hole, and F_{array} is the field at the hole in the presence of the array divided by that for an isolated hole.

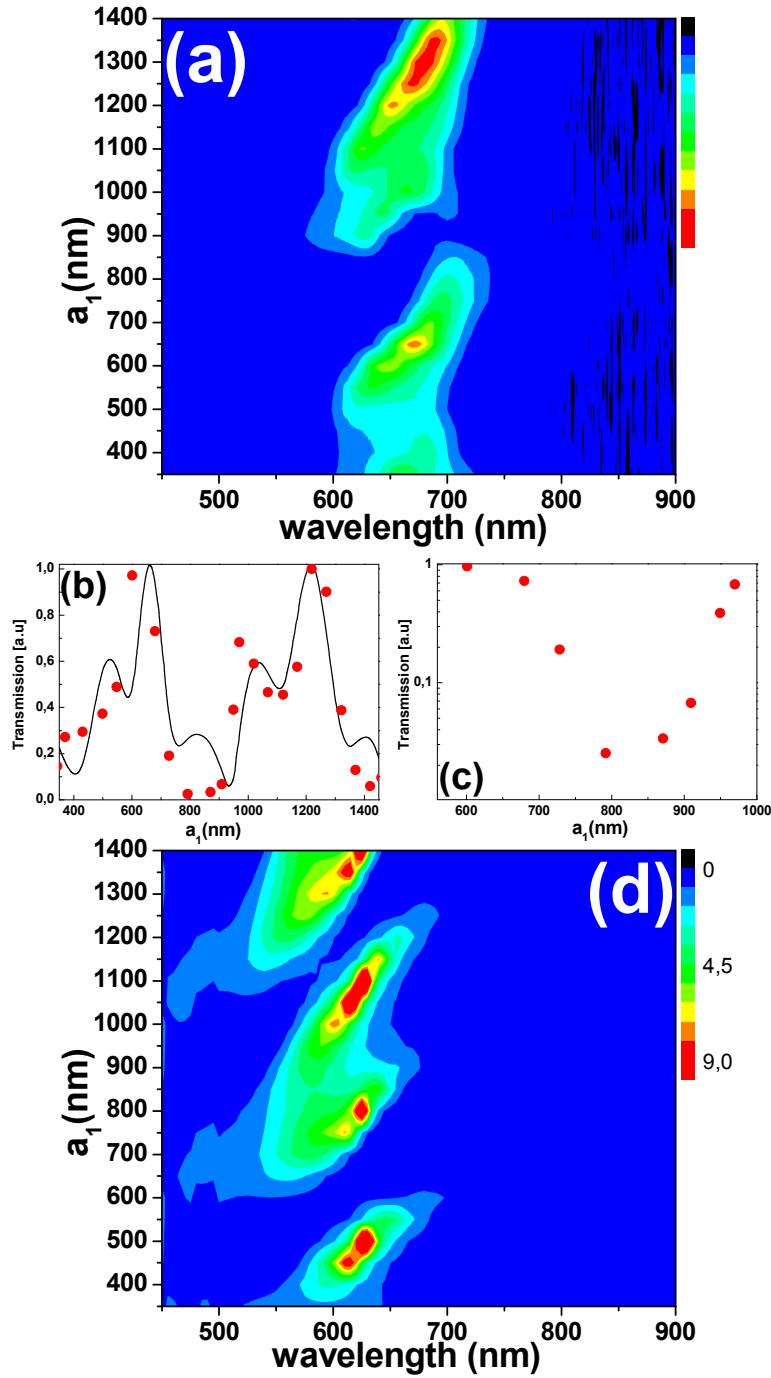


Fig. 2. (a) Optical transmittance for the considered bull's eye with $N = 6$ annular grooves, $h = 280\text{nm}$, $h_g = 90\text{nm}$, $w_g = 220\text{nm}$ and $r_c = 125\text{nm}$. The spectra are acquired as a function of both distance between the hole and the first groove, a_1 , and incident wavelength λ . The color scale is linear and in arbitrary units. (b) Experimental transmittance collected at $\lambda \simeq 660\text{ nm}$ as a function of a_1 , normalized to the transmission maximum. The continuous line is a fit from the phenomenological model of Eq.(1) with fitting parameters discussed in the text. (c) Zoom of the results in panel (b) over a smaller region of a_1 values, in logarithmic scale. (d) CMM calculations for the transmission of light normalized to hole area.

Under these conditions, the re-illumination term can be expressed in terms of the (complex valued) SP wavevector k_{sp} as

$$F_{array} \approx 1 + \gamma\sqrt{a_1} e^{(ik_{sp}a_1)} + r\gamma\sqrt{a_1} e^{(3ik_{sp}a_1)} \quad (1)$$

The first term represents the incident EM field, the second one accounts for the light mediated by SP going directly from the groove array to the central hole, whereas the third term represents the light that goes from one side of the “black box” to the other one, and then is reflected back to the central hole. In principle, the parameters γ and r are expected to depend smoothly on a_1 and λ but, as the exact dependence is unknown, they will be initially considered as constants. Only a full numerical calculation will be able to define these parameters properly and to evaluate their exact dependencies, along with the role played in enhanced transmission by the different EM couplings between BE elements -see below. In Eq.(1), the cylindrical symmetry has been accounted for by considering the SP as planar cylindrical waves. For a propagation over a distance x , the field amplitude associated to a SP locally launched at the level of the cylindrical groove is proportional to $e^{(ik_{sp}x)}/\sqrt{x}$. The total field amplitude will scale as \sqrt{x} after integrating over the whole cylindrical groove, explaining the $\sqrt{a_1}$ dependency in Eq. (1).

Figure 2(b) shows a fit of the transmittance obtained at $\lambda = 660\text{nm}$ with this phenomenological model for $|\gamma| = 0.014$ and $|r| = 0.65$. The same beating when a_1 is varied is found for other wavelengths around $\lambda = 660\text{nm}$. This fit allows interpreting the observed spectral resonances which arise from the interference between (i) the field directly re-routed by the grooves into the hole and (ii) the field re-routed by one side of the array that, before reaching the hole, suffers a reflection at the other side of the array. The contribution (i) essentially selects a_1 values corresponding to the transmission resonances that dominate the transmission spectra in a standing-wave pattern (c.a. every $\lambda_{SP}/2$) while (ii) is responsible for the secondary transmission peak at $a_1 \sim 990\text{nm}$. In other words, the optical spectra acquired in the $\lambda - a_1$ parameter space are revealing unambiguously the coherent character of the BE structure which can therefore be envisioned as a genuine sub-micron SP cavity. Controlling the optical transmission is therefore possible through the choice of a_1 values. Figure 2(c) demonstrates a selective modulation of the transmission of almost 2 orders of magnitude. The dephasing between the SP component and the direct transmission through the hole is thus directly related to the cavity radius. At a specific value of a_1 , the two components can destructively interfere, leading to a strong suppression of the transmission signal as displayed in Fig. 2(c). The recently shown SWEDA effect is based on the same discussion with similar interference effects at play within the BE cavity [14].

3. Numerical results and theory

In order to go beyond this phenomenological model, we have carried out numerical calculations based on the Coupled Mode Method (CMM) [26]. Within the CMM, the EM fields are expanded in terms of eigenmodes in each different region in space (plane waves in the semi-infinite regions and waveguide modes inside the hole and grooves). Imposing the appropriate matching conditions leads to a coupled system of equations for the modal amplitudes of the electric field at the entrance, E , and at the exit, E' , of the cavities. In the case of subwavelength holes or grooves, considering only one mode per cavity (the TE_{11} mode in both the hole and the grooves [25]) already provides a good approximation to the transmission properties [2, 26]. In this case, the modal amplitudes are governed by:

$$\begin{cases} -\sum_n E_n + \sum_m G_{nm} E_m = I_n + G_n^y E_n' \\ -\sum_n E_n' + \sum_m G_{nm} E_n' = G_n^y E_n \end{cases} \quad (2)$$

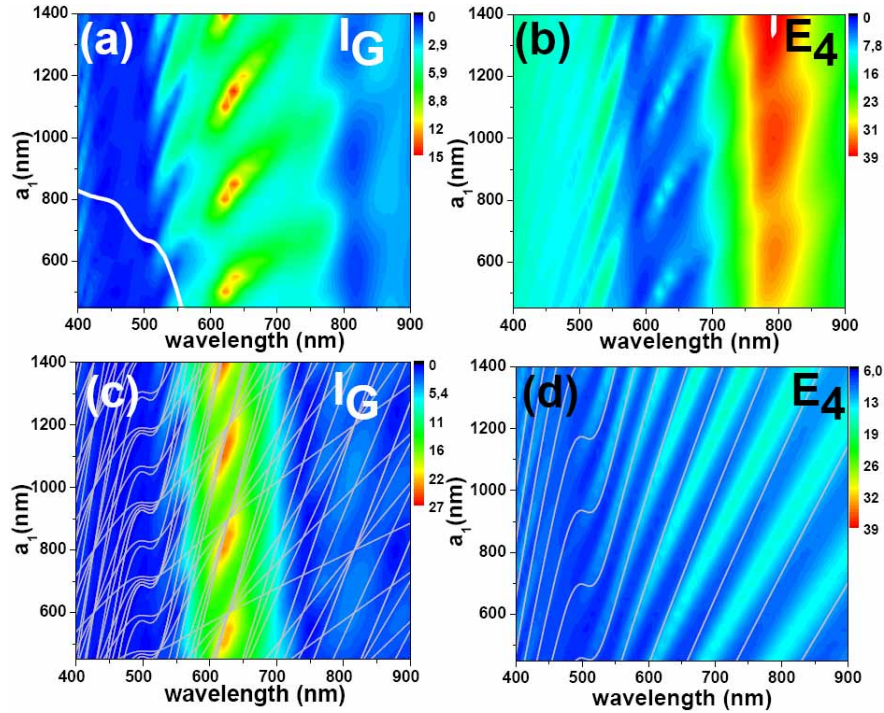


Fig. 3. For the geometrical parameters in Fig. 2, computed re-illumination from the grooves in the central hole (panel (a)) and amplitude of the electric field at the entrance of the fourth annular groove $|E_4|$ (panel (b)), as a function of a_1 and λ . Panels (c) and (d) show the same as panels (a) and (b), respectively, but for a system of “disconnected” grooves, i.e. by setting $G_{nm} = 0$ for $n \neq m$. Grey lines depict the condition $2a_n = m_n \lambda_{SP}$ for each annular groove. The white line in panel (a) renders the spectral dependence for the transmittance through a single hole ($\times 1000$).

where n is an index that labels cavities ($n = 0$ for the hole, and $n = 1 \dots N$ for the grooves).

The CMM method provides analytical expressions and a physical interpretation for all the objects in the system above (see Ref. [26, 27] for further details): I_n accounts for the external illumination impinging directly on the grooves or holes; Σ_n represents the light that comes back to the aperture after bouncing back and forth inside the cavities, and the term G_n^v is linked to the coupling of EM fields at the two sides of the film through the holes. Finally, G_{nm} represents the EM coupling between different apertures, mediated by diffraction modes.

As a technical note, in the simulations we apply surface impedance boundary conditions (SIBC) [28] at the horizontal surfaces for the dielectric response of the metal. For each cavity (groove or hole) the propagation constant along the vertical direction is computed exactly. The spatial profile of the fundamental waveguide mode is obtained considering perfect electrical conductor approach in the waveguide since, in this case, the overlap with plane waves is known analytically [25]. Based on our experience on 1D structures, where due to the higher symmetry the obtained results can be compared with virtually exact numerical simulations, we expect that the use of this approximation rigidly blue shifts the transmission spectra by ≈ 50 nm.

3.1. Bull's eye response

Figure 2(d) renders the transmittance (normalized to the hole area) computed within the CMM for the nominal parameters of the experimental setup. The dielectric constant for gold is taken from the experimental values tabulated for a clean metal surface in Ref. [29]. Due to this fact we expect that the theoretical calculations for transmission will be overestimated as compared to those obtained experimentally, since in the FIB process, absorption in gold may increase. The simulations also present stripes of enhanced optical transmission in the $\lambda - a_1$ parameter space, appearing around $\lambda_R = 630\text{nm}$, i.e., within the expected accuracy of the model, and with a difference of about 100nm in a_1 values which we attribute to possible imperfections and deviations from nominal parameters of the fabricated structures, but also to the approximations done within the CMM formalism.

One of the main advantages of the CMM formalism is that it allows us to differentiate amongst different mechanisms involved in the transmission process. For instance, we have considered BE structures with and without a central hole. We have found that the amplitude of the electric field at the entrance of the grooves, E_n , is not affected by the presence of the central hole, making evident that, for the range of parameters considered, the cross-section of the hole is much smaller than those of the grooves. This result indicates that, at a given wavelength, it is possible to analyze separately the optical responses of the array and the central hole, justifying one of the assumptions of the phenomenological model described above.

To obtain additional insight on the effect of the array, Fig. 3 shows the computed maps for the light going from the groove array to the central hole, I_G (panel (a)) and the amplitude of the electric field at the entrance of the fourth groove, $|E_4|$ (panel (b)), which is taken as a representative illustration of the field at the surface. In the spectral band close to λ_R both I_G and $|E_4|$ present hot spots with locations in the $\lambda - a_1$ plane that coincide with those of the transmittance. However, for wavelengths larger than the cutoff of the hole (which, for the parameters considered occurs at $\lambda_c \approx 589\text{nm}$), both I_G and $|E_4|$ present spectral features that are not observed in the total transmittance, as the latter is strongly suppressed by the small transmittance of the central hole. Notice that $|E_4|$ presents an even stronger resonance at $\lambda \approx 800\text{nm}$ than at λ_R . Actually, the calculations show that *all* grooves present a resonant electric field at the same wavelength, pointing to a collective behavior. However, this resonant field does not lead to a resonant I_G , because the fields radiated by the grooves do not interfere constructively at the centre of the structure. We have found (not shown here) that when the groove depth increases, the collective resonance enhances and red-shifts, whereas the one at λ_R also increases in intensity but its spectral position remains invariable.

To understand the origin of the “hot stripes” in I_G and E_n that lead to EOT, we now consider the response of a set of isolated annular grooves (by simply setting $G_{nm} = 0$ for $n \neq m$). Panels (c) and (d) in Fig. 3 show the same calculations as in panels (a) and (b), respectively, but when grooves are “disconnected”. The re-illumination map when grooves do not interact presents a similar pattern to that of I_G when the full interaction is considered: there are high intensity features at $\lambda_R \approx 630\text{nm}$ only for some values of a_1 . This result clearly shows that maxima in I_G originate from the constructive interference at the hole of the EM fields radiated by each groove (I_g) which, at those wavelengths, can be considered as isolated. The comparison between $|E_4|$ in the connected (Fig. 3(b)) and isolated cases (Fig. 3(d)) reinforces this interpretation: in the spectral region close to λ_R , where the resonance in both I_G and T occur, $|E_4|$ is similar for both an isolated and a “connected” groove. In contrast, these two situations lead to very different $|E_4|$ in the resonance appearing at $\lambda \approx 800\text{nm}$, adding further evidence to the association of this resonance to a collective behavior.

From now on we concentrate on the spectral region close to λ_R , where the transmission resonances occur. The previous analysis show that, in this case, the grooves can be considered

as independent of each other. We find that an isolated shallow groove (with $h \ll \lambda$, as those considered in this work), re-illuminates the centre of the structure maximally when an integer number of SP wavelengths fits inside each ring cavity, that is, $2a_n = m_n \lambda_{\text{SP}}$, where m_n is an integer and a_n is its average radius. This is consistent with the fact that, in the optical regime and at distances larger than $2 - 3\lambda$, SP are the main contribution to the EM field at the surface radiated by a surface defect [30,31]. This condition is represented by the grey lines in Fig. 3(d) for the fourth groove, and as a collection of straight lines in Fig. 3(c), one for each groove ($n = 1, \dots, 6$). Notice that in Fig. 3(c) all lines cross at several points, where the re-illumination from each groove is maximal simultaneously. For a collection of grooves with average radius $a_n = a_1 + (n - 1)p$, where n does not necessary have to be consecutive (eventually providing aperiodic structures), these maximal points are given by the conditions

$$\lambda_{\text{SP}} \approx \frac{p}{l} \quad (3)$$

$$a_1 \approx m \frac{\lambda_{\text{SP}}}{2} \quad (4)$$

where m and l are integers. Moreover, all partial re-illuminations interfere constructively in that case. This explains the maximum in I_G that occurs in both the disconnected case (Fig. 3(c)) and the connected one (Fig. 3(a)). The small deviation between the actual values of a_1 and λ for maximum I_G and those given by Eq. (3) and Eq. (4) are due to the influence of both groove width and, principally, groove depth which are not taken into account in the simple model outlined above. Actually, considering h_g enlarges the optical path length that light must cover which eventually translates into a larger effective \tilde{a}_1 . Therefore, grey lines in Fig. 3 intersect at larger a_1 values than those where actual hot spots in the reillumination process, occur. In the limit of very shallow grooves, hot spots and the intersection of grey lines coincide (results not shown here).

These scaling laws are in good correspondence with experimental results. Main resonances shown in Fig. 2 appear at $\lambda = 660\text{nm}$, very close to λ_R , as it is predicted by Eq. (3) for $l = 1$, but they also obey Eq. (4), with $m = 1, 2, 3, 4$, in the range of parameters here studied. In order to stress the importance of following this set of simple equations when designing BE structures, we also conducted the experiments appearing in Fig. 4. This figure shows transmission spectra and the expected resonant wavelengths λ_R for BE structures with different geometrical parameters (see caption) with $a_1 = p$ for different periods. Again the difference between the simple prediction and the experiment is attributed mainly to the influence of groove depth. Note that these λ_R values are calculated from $\text{Re}[k_{sp}[\lambda_R]] = 2\pi/(p/l)$, being $l = 2$, and that a_1 values are properly selected with $m = 4$. This draws a straightforward analogy with periodic hole arrays where higher order SP modes can be excited at specific wavelength in agreement with a grating law of the kind of Eq. (3). To our knowledge, such measurements have never been presented to date on a BE structure.

As said before, the CMM provides analytical expressions for all objects appearing in Eq. (2) which, in principle, have to be evaluated numerically. However, we find that, to a very good approximation, the elements G_{nn} and G_{0n} (related to how a groove re-illuminates itself or the central hole, respectively) satisfy:

$$\begin{aligned} G_{0n}(a_n) &= \sigma(a_n) e^{ik_{sp}a_n} \\ G_{nn}(a_n) &= \beta(a_n) + \Gamma(a_n) e^{2ik_{sp}a_n} \end{aligned} \quad (5)$$

where $\sigma(a_n)$, $\beta(a_n)$, and $\Gamma(a_n)$ are fitting complex coefficients that depend *smoothly* on a_n . Equation (5) can be interpreted physically in the following way: the groove re-illuminates the

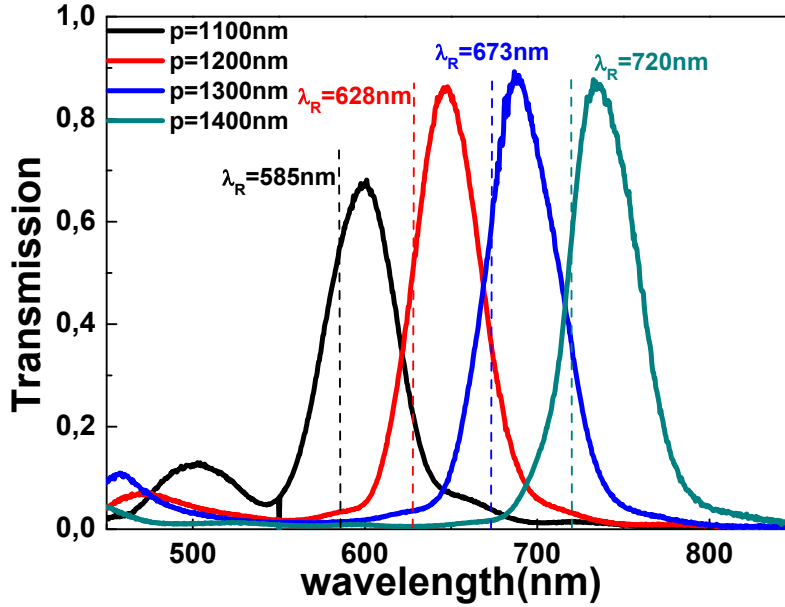


Fig. 4. Transmission spectra measured through BE structures with $N = 5$, $h = 280\text{nm}$, $h_g = 90\text{nm}$, $w_g = 330\text{nm}$, $r_c = 170\text{nm}$, and different periods (see label) being $a_1 = p$. For each period, the predicted location of λ_R is indicated. These wavelengths follow Eq. (3), so that $\text{Re}[k_{sp}[\lambda_R]] = 2\pi/(p/l)$, being $l = 2$, and Eq.(4) with $m = 4$.

hole via SP while, for the self re-illumination, the groove can be considered as composed by two parts (left and right). These parts re-illuminate themselves (leading to the $\beta(a_n)$ contribution) and one another (the $\Gamma(a_n)$ term).

3.2. Isolated groove response

Since the previous analysis indicates that the array response can be understood as the response of isolated grooves, let us now consider an isolated groove with the same h_g and w_g as before and of average radius a . To simplify the notation, we write $G_{0n} = G_0(a)$ and $G_{nn} = G(a)$. As an illustration of the validity of Eq. (5), Fig. 5 shows $|G_0(a)|$ and $|G(a)|$ calculated both exactly (using Eq. (2)) and fitted through Eq. (5), together with $|\sigma(a)|$, $|\beta(a)|$, and $|\Gamma(a)|$ obtained from the fit. This illustration is for the geometrical parameters considered in this paper and $\lambda_R = 630\text{nm}$, but we have checked that the validity of Eq. (5) is not restricted to these particular case.

Equation (5) also allows for a simplified analysis of the re-illumination process of a single groove, $I_g(a) = G_0(a)E(a)$, which can be written in the language of the Huygens-Fresnel model [32]. Equation (2) in combination with Eq. (5) gives

$$E(a) = \frac{I(a)}{G(a) + \Sigma(a)} \approx \frac{I(a)}{\beta(a) + \Sigma(a)} \cdot \frac{1}{1 - r(a)e^{2ik_{sp}a}} \quad (6)$$

where

$$r(a) \equiv \frac{-\Gamma(a)}{\beta(a) + \Sigma(a)} \quad (7)$$

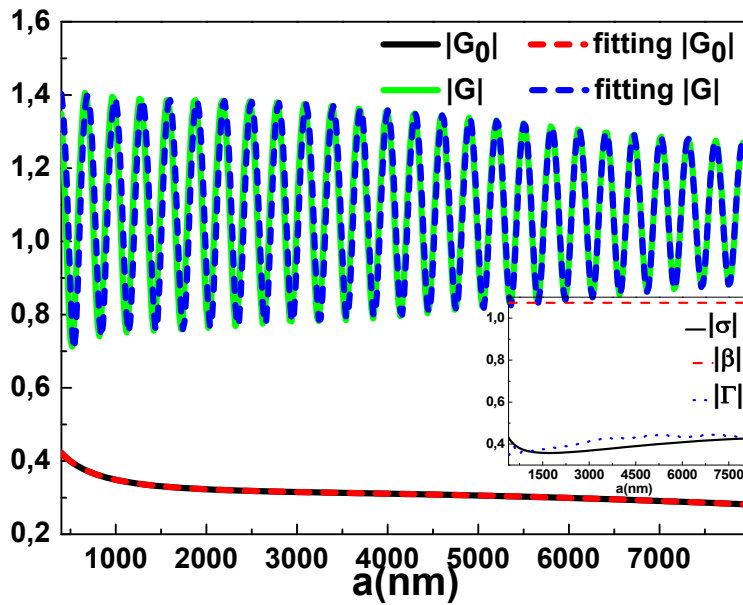


Fig. 5. For the geometrical parameters in Fig. 2 and $\lambda_R = 630\text{nm}$, comparison between the exact values for $|G_0|$, $|G|$ obtained directly from Eq. (2), and those fitted using Eq. (5), as a function of a . The inset shows $|\sigma(a)|$, $|\beta(a)|$, and $|\Gamma(a)|$ values as a function of a .

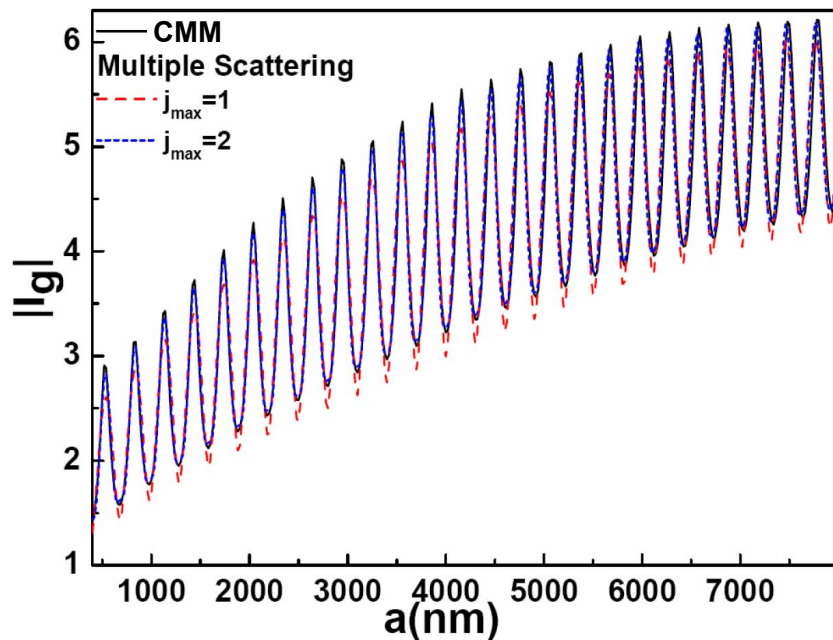


Fig. 6. Reillumination of a single groove, $|I_g|$, as a function of a . The black curve represents the exact calculations obtained directly from Eq. (2). The blue and red curves show the result after fitting $\alpha(a)$ and $r(a)$ and truncating the sum in Eq. (9) to $j_{max} = 1$ and 2 terms, respectively. Geometrical parameters as in Fig. 3 and $\lambda_R = 630\text{nm}$.

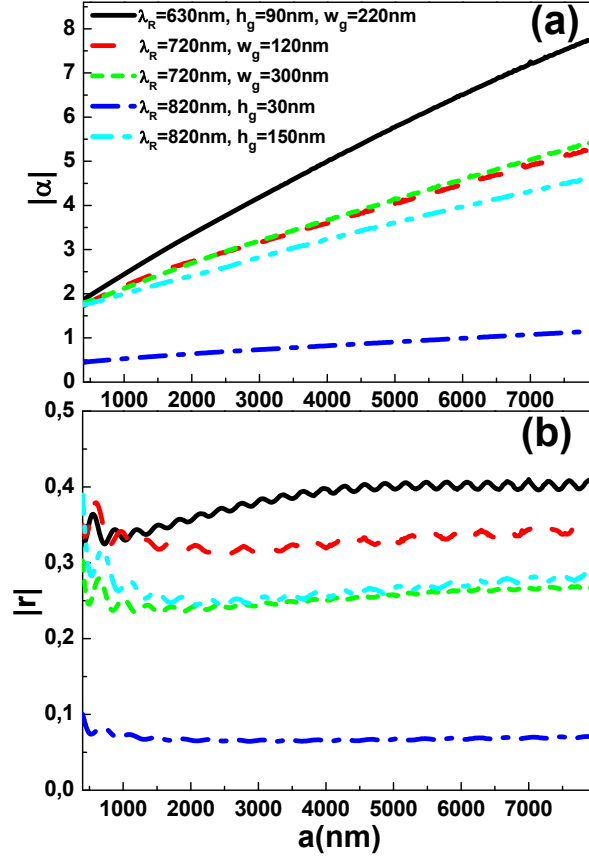


Fig. 7. Calculation (within the CMM model) for $\alpha(a)$ (panel (a)) and $r(a)$ (panel (b)) for different set of parameters. The black curve is for the system considered in Fig. 2, which is taken as the reference. For the other cases, the labels give the parameters that are different from those in the reference.

Expanding the denominator we get:

$$E(a) = \frac{I(a)}{\beta(a) + \Sigma(a)} \sum_{j=0}^{\infty} [r(a) e^{2ik_{sp}a}]^j \quad (8)$$

Notice that this expression contains the “multiple scattering” between the left and the right side of the annular groove. Finally, if we substitute the latter in $I_g(a) = G_0(a)E(a)$, we obtain:

$$I_g(a) = \alpha(a) e^{ik_{sp}a} \sum_{j=0}^{\infty} [r(a) e^{2ik_{sp}a}]^j \quad (9)$$

with

$$\alpha(a) \equiv \frac{\sigma(a)I(a)}{\beta(a) + \Sigma(a)} \quad (10)$$

Figure 6 shows the exact results for $I_g(a)$ and the fitted curve replacing $\alpha(a)$ and $r(a)$ in Eq. (9). The excellent agreement between the two calculations confirms the validity of the approximations involved in the derivation of the simplified model. Note also that considering just the first two terms ($j_{max} = 1$) in the sum in Eq. (9) already provides a good approximation.

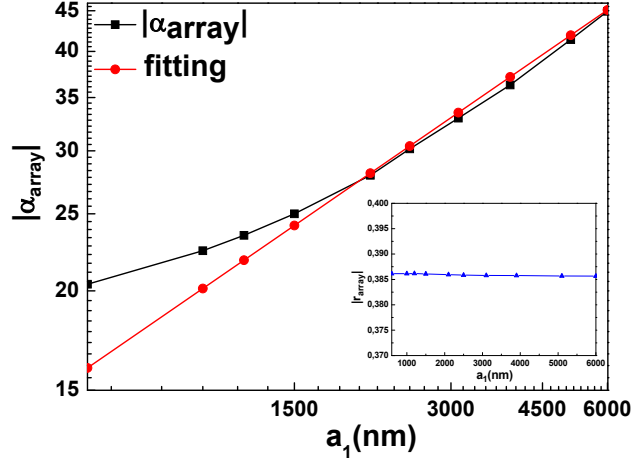


Fig. 8. Calculation (within the CMM model) in logarithmic scale for α_{array} as a function of a_1 for the same geometrical parameters as in Fig. 2 at $\lambda_R = 630\text{nm}$. The black curve represents calculations from Eq. (12) and the red one, the fitting curve where $|\alpha_{array}| \sim a_1^x$ with $x = 0.45$. The inset shows the corresponding calculations for $|r_{array}|$.

In Fig. 7 we plot the coupling and reflection coefficients for the groove parameters previously considered (continuous black curves). Additionally, we present results for other representative geometries still in the subwavelength regime, which result from the one considered throughout this paper by increasing and decreasing some geometrical parameters (and, in each cases, for the corresponding values of λ_R). These results show that, in all cases, the coupling amplitude α increase with groove radius, while the reflection amplitude r is practically independent of a . The dependence of α with a can be approximately fitted to $\alpha(a) \propto a^{2/3}$. This result, which is relevant to studies in BE structures based on the Huygens-Fresnel approach, can be traced back to arise from the exact $a^{1/2}$ dependence of $I(a)$ (i.e., the illumination of a groove is proportional to its area), plus an additional dependence with a of the coefficients entering Eq. (5) (see inset in Fig. 5). The computed reflection coefficient turns out to be smaller than the one given by the phenomenological model ~ 0.65 (which can only be helpful in an interpretation context). These studies also suggest that the width of the groove is not a parameter with a strong influence on the results (provided it is in the subwavelength regime).

In the spectral region where transmission resonances occur (where grooves can be treated independently), we can obtain the total re-illumination at λ_R provided by an array of grooves placed at a_n as $I_G = \sum_n I_g(a_n)$. Thus, following Eq. (9)

$$I_G = \alpha_{array} e^{ik_{sp}a_1} \left(1 + r_{array} e^{2ik_{sp}a_1} \right) \quad (11)$$

with

$$\begin{aligned} \alpha_{array} &= \sum_n \alpha(a_n) e^{ik_{sp}(n-1)p} \\ r_{array} &= r \cdot \frac{\sum_n \alpha(a_n) e^{3ik_{sp}(n-1)p}}{\sum_n \alpha(a_n) e^{ik_{sp}(n-1)p}} \end{aligned} \quad (12)$$

where, according to Fig. 6 and Fig. 7, the reflection coefficient r is assumed to be independent of a_1 , and $j_{max} = 1$. Additionally, if the condition $p \cdot \text{Re}[k_{sp}] \approx 2\pi l$ (being l an integer) is

fulfilled, which is also the condition for validity of the independent-groove model, $r_{array} \approx r$ and $\alpha_{array} \approx \sum_n \alpha(a_n)$.

In the CMM formalism, $F_{array} = 1 + I_G/I_0$, so Eq. (11) recovers the phenomenological model given by Eq. (1). Moreover, in Fig. 8 we show $|\alpha_{array}|$ as a function of a_1 for the same geometrical parameters considered in Fig. 2 at $\lambda_R = 630\text{nm}$. Notably, we find for large a_1 values that $|\alpha_{array}|$ behaves as $a_1^{0.45} \sim \sqrt{a_1}$, as predicted by the simple phenomenological model. Note also that, despite the slow dependence of α_{array} with a_1 , the reillumination at the centre of the hole strongly oscillates with a_1 , due to the exponential terms in Eq. (11). Additionally, inset in Fig. 8 shows that $|r_{array}|$ hardly depends on a_1 , as it was expected from Fig. 7.

4. Conclusions

We have analyzed the optical transmission in bull's eye structures as a function of the distance between the central hole and its nearest groove, a_1 , in the case when all groove depths and widths are subwavelength. We have shown that the transmittance presents maxima for given values of a_1 and wavelength, which are due to constructive interference of the light reemitted by grooves (which in that case behave almost independently) into the central hole. This reemitted light is in the form of surface plasmons. Furthermore, each groove acts as two connected cavities and, for fully explaining the transmittance spectra, the reflection by one cavity of the surface plasmon radiated by the other cavity must be taken into account. We have shown that the amplitude for coupling of incident radiation into a groove increases with groove radius, while the reflection coefficient of a groove for surface plasmons does not. These ingredients have been combined to give a simple Huygens-Fresnel view of the total coupling and reflection of light by the groove array. Finally, our results show that there is not a direct correspondence between field enhancement at the surface and transmission enhancement, as there are resonances in the groove array that do not lead to strong re-illumination at the central hole.

Acknowledgments

We acknowledge the support from the Spanish Ministry of Science and Innovation (the projects MAT2008-06609-C02 and CSD2007-046-Nanolight.es) and the support from the ERC (Grant 227557).